

NOISE STABILIZED RANDOM ATTRACTOR

J. M. Finn*, E. R. Tracy**, W. E. Cooke**, and A. S. Richardson**

8th November 2018

*T-15, Plasma Theory, Los Alamos National Laboratory; **Department of Physics, College of William and Mary

Abstract

A two dimensional flow model is introduced with deterministic behavior consisting of bursts which become successively larger, with longer interburst time intervals between them. The system is symmetric in one variable x and there are bursts on either side of $x = 0$, separated by the presence of an invariant manifold at $x = 0$. In the presence of arbitrarily small additive noise in the x direction, the successive bursts have bounded amplitudes and interburst intervals. This system with noise is proposed as a model for edge localized modes in tokamaks. Further, the bursts can switch from positive to negative x and vice-versa. The probability distribution of burst heights and interburst periods is studied, as is the dependence of the statistics on the noise variance. The modification of this behavior as the symmetry in x is broken is studied, showing qualitatively similar behavior if the symmetry breaking is small enough. Experimental observations of a nonlinear circuit governed by the same equations are presented, showing good agreement.

1 Introduction

This paper is motivated by observations of extreme noise sensitivity in a two-dimensional flow of the form

$$\frac{dx}{dt} = f(x, y) \equiv (y - 1)x, \quad (1)$$

$$\frac{dy}{dt} = g(x, y) \equiv \epsilon y^\nu - x^2 y. \quad (2)$$

This system is a low-dimensional model for the nonlinear behavior of a plasma instability in which y represents the pressure gradient, and instability (with amplitude x) is driven by the pressure gradient and fixed magnetic field line curvature. Such pressure -driven instabilities are thought to be responsible for edge localized modes (ELMs) observed as fluctuations at the edge of a tokamak [1, 2]. Some ELMs, called Type-I ELMs, show temporal behavior which is quite simple, consisting of well separated large bursts, indicating that their dynamics can be represented by a low-order system. However, the time series appear to show chaos, and it is of some interest to determine whether this apparently chaotic behavior is indeed deterministic chaos or whether it is due to sensitivity to noise from, for example, the plasma core. For example, if the apparent chaos is due to noise, the behavior can occur in a two dimensional model, whereas an autonomous model showing similar apparently chaotic behavior must be at least three dimensional.

The effect of noise has been studied in other experimental physics situations, and the kind of extreme sensitivity to noise we discuss here has been observed. For example, in experiments involving the formation of droplets in a viscous fluid[3], the fluid is observed to form thin necks repeatedly as a part of the process. Simulations showed the formation of necks, but the *repeated* formation of necks required noise in the modeling, although extremely small noise gave agreement. Another example involves studies of a Nd:YAG (neodymium doped yttrium aluminum garnet) laser with an intercavity KTP (potassium titanyl phosphate) crystal. Theoretical studies were performed to model the laser dynamics[4], showing that the type-II chaotic dynamical behavior of the laser was observed to be very sensitive to noise and was actually found to amplify the noise. Because of

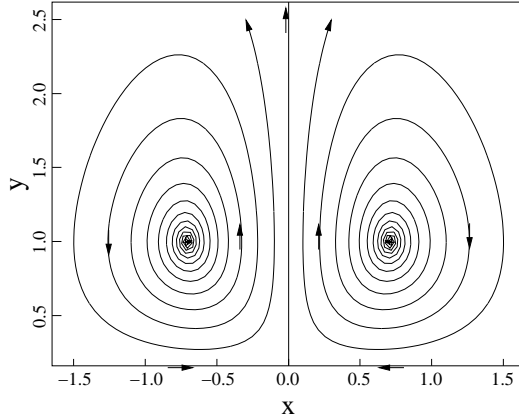


Figure 1: Orbits initiated near the fixed points at $x = \pm x_0 = \pm\sqrt{\epsilon}$, $y = 1$. The orbit on the right spirals out clockwise, the one on the left counter-clockwise. The x - and y -axes are, respectively, stable and unstable manifolds of the fixed point at the origin.

the role of a very low level of noise in such disparate physical systems, we have been motivated to do detailed studies of (1), (2) and related systems perturbed with a low level of noise.

For the system (1), (2) with zero noise, x grows if $y > 1$, but for large enough x the term $-x^2y$, which represents the flattening of the pressure gradient due to the fluctuation, enters. This causes a decrease in y , which quenches the growth. For this flow, $x = 0$ is an invariant manifold, and is in fact the unstable manifold of a fixed point at $x = y = 0$. See Fig. 1. The x -axis is also an invariant manifold, the stable manifold of the same fixed point. There are two unstable spirals with $x = \pm x_0 = \pm\sqrt{\epsilon}$. The nonlinear deterministic behavior consists of spirals coming out of the fixed points with $x = \pm x_0$, coming closer to the two invariant axes on each pass, and developing increasingly larger bursts, one for each encircling of the spirals, more widely separated in time. Because of symmetry in x , identical bursts can occur on both sides of $x = 0$, isolated from each other by the invariant manifold $x = 0$.

With a small amount of uncorrelated Gaussian noise added to eq. (1), we find that the resulting nonlinear stochastic equation has the following property: the bursts saturate in amplitude, leading to behavior that is qualitatively similar to deterministic chaos. We call this behavior *noise-stabilization*. Further, the noise allows transitions across the y -axis, an invariant manifold for the

deterministic system. Statistically, the dynamics is symmetric. In particular, we focus on the fraction of the number of bursts with $x < 0$ compared with those with $x > 0$; with statistical symmetry these are equal. In the physical system motivating this work, the processes we model as noise have a much shorter correlation time than the processes described by the deterministic equations (1), (2), hence modeling them as noise is appropriate. Noise-stabilized systems are interesting for several reasons. Most importantly, although they can exhibit dynamical behavior that is reminiscent of deterministic chaos, it is likely that their behavior for very low noise level is distinguishable from deterministic autonomous low dimensional systems. Our model system was chosen to emphasize the noise-stabilizing effect, in the sense that it has no attractor in the zero noise limit. In physical applications, distinguishing noise-stabilized behavior from more familiar types of dynamics could be critical for understanding and predicting how the system under study will change as the noise driving is modified.

There have been several related papers on nonlinear stochastic equations which are sensitive to a small amount of noise. Sigeti and Horsthemke [5] studied the effect of noise at a saddle-node bifurcation, and found noise induced oscillations at a characteristic frequency. Stone and Holmes [6] studied systems with an attracting homoclinic orbit or an attracting heteroclinic cycle (structurally stable because of the presence of a symmetry) in the presence of noise. They found that the effect of the noise is to prevent the time between bursts from increasing on each cycle. Stone and Armbruster [7] studied structurally stable (again because of symmetry) heteroclinic cycles in the presence of noise, and analyzed the jumping between invariant subspaces of the deterministic system. Armbruster and Stone [8] studied heteroclinic networks in the presence of noise, and the induced switching between cycles. References [6, 7, 8] stressed the importance of the linear part of the flow near the saddles. Moehlis [9] has investigated a system representing binary fluid convection, and found that states with large bursts can be very sensitive to noise. References [10, 11] deal with a system (SEIR or susceptible-exposed-infected-recovered) describing epidemic outbreaks and show that chaos can be induced for parameters far from the region for which the deterministic system is chaotic.

The difference between our work and this previous work is the following. Our work concerns a system which, in the absence of noise, has successive bursts, each larger than its predecessor and separated by lengthening time intervals. In the presence of noise, our system exhibits a finite characteristic scale for the burst amplitude, a characteristic time for bursts, and random switching across an invariant manifold of the deterministic system. Further, our deterministic system is two-dimensional, and therefore cannot have deterministic chaos, but the noise introduces behavior which resembles deterministic chaos in several ways. In Refs. [6, 7, 8] systems with homoclinic or heteroclinic cycles were studied; the noise was found to induce switching between subspaces and introduced a characteristic time scale for intervals between bursts, but the bursts in the deterministic system were limited in magnitude. The model of Ref. [9] is four-dimensional, and therefore can, unlike our system, exhibit chaotic behavior even without noise, in principle. It was found that this specific system can have periodic bursts of infinite magnitude. These infinite bursts are periodic in the sense that if the origin and infinity are mapped to each other in a specific way, the solutions to the equations can reach the origin in finite time and can be integrated through it, leading to a periodic signal. These states with large periodic bursts were found to be sensitive to noise. This behavior is to be contrasted with the behavior we have found from eqs. (1), (2), in which (for $\nu < 2$) successive bursts get larger in magnitude, but no single burst goes to infinity, and noise causes the bursts to behave in a way that resembles deterministic chaos. The model in Refs. [10, 11] exhibits noise-induced chaos because of bi-instability, related to the presence of two nearby unstable orbits.

The model we introduce is similar to the models of Refs. [6, 7, 8] with a heteroclinic connection, in the formal sense that in our model the y -axis is a heteroclinic orbit between the saddle at $(x, y) = (0, 0)$ and the point at infinity. After a change of variables, the point at infinity can be mapped to a finite point and the origin can be left fixed. The new unstable manifold maps from the origin to this second fixed point. However, additive noise in our system would then map to non-additive noise in the compactified version. In particular the noise disappears at the second fixed point, which is physically unrealistic.

In Sec. 2 we introduce the deterministic form of the model and show that with $\nu = 1$ it is

equivalent to the Lotka-Volterra predator-prey model. We discuss the surface of section map $x \rightarrow x' = F(x)$, taking minima of x to maxima of x (and vice-versa), as well as the composite map $x \rightarrow x''$.

In Sec. 3 we introduce the stochastic model and present results. These results include those on the Lyapunov exponent h_1 and the distribution of maxima of $|x|$ and the time interval T between bursts, and the dependence of these quantities on the noise diffusion coefficient D . A brief discussion of the behavior near the y -axis is shown. In this limit, the behavior in x is linear and can be treated by the Fokker-Planck equation, discussed in more detail in Appendix A.

In Sec. 4 we discuss the role of reflection symmetry in x and the effect of weak symmetry breaking. We also present results involving modifications to the system at small and large y , and a modified form of the equations in which the noise is replaced by a sinusoidal perturbation. The results with an offset show that in a sense the system with noise is structurally stable. The results with a sinusoidal perturbation lend credence to the validity of the Lyapunov exponent for the random case.

In Sec. 5 we show results from an experiment with a nonlinear circuit, showing noise stabilization in a physical system.

In Sec. 6 we summarize our work.

2 Deterministic model

The deterministic form of the model we study is eqs. (1), (2). The parameters ϵ , ν are the only parameters that cannot be removed by rescaling x , y , and t . Starting with $x = 0$ and $y > 0$, y increases in time, going to infinity in finite time if $\nu > 1$. For $y > 1$ small initial values of x begin to grow. [The instantaneous growth rate of x in (1) equals $y - 1$.] If x grows at a rapid enough rate relative to y (to be quantified later), the second term in (2) eventually dominates the first and y decreases. For $\nu = 1$ the system (1), (2) is the Lotka-Volterra predator-prey model. The usual

form[12] of this system, in scaled variables, is

$$\begin{aligned}\frac{dX}{ds} &= X(Y - 1), \\ \frac{dY}{ds} &= (E - X)Y.\end{aligned}$$

With the change of variables $X = x^2/2$, $Y = y$, $s = 2t$, $E = \epsilon/2$, it can be put in the form of eqs. (1), (2) with $\nu = 1$. Notice that in this latter form there is a symmetry $x \rightarrow -x$ not present in the usual form. For this value of ν , equations (1) (2) can be written in terms of $q = \ln x$, $p = \ln y$ in the form

$$\begin{aligned}\frac{dq}{dt} &= e^p - 1, \\ \frac{dp}{dt} &= \epsilon - e^{2q}.\end{aligned}$$

Thus eqs. (1), (2) are an autonomous Hamiltonian system, with canonical variables (q, p) :

$$H(q, p) = e^p - p + \frac{1}{2}e^{2q} - \epsilon q = y - \ln y + \frac{1}{2}x^2 - \epsilon \ln x. \quad (3)$$

Successive intersections of $H = \text{const.}$ with $y = 1$ define a 1D surface of section map $x \rightarrow x' = F(x)$. See Fig. 2. There are centers at $x = \pm x_0 = \pm\sqrt{\epsilon}$, $y = 1$. The mapping F is determined from $H(q, p)$, i.e.

$$\frac{1}{2}x^2 - \epsilon \ln x = \frac{1}{2}x'^2 - \epsilon \ln x'. \quad (4)$$

For small x we find $x \approx x' \exp(-x'^2/2\epsilon)$, which can be approximated further by $x' = \sqrt{-2\epsilon \ln x}$. Thus for small x or very large x' , $F(x)$ is logarithmic in nature. For large x or small x' we have the inverse $x' = x \exp(-x^2/2\epsilon)$.

On the other hand, for $\nu > 1$ the system is not Hamiltonian. It has fixed points at $y = 1$, $x = \pm x_0 = \pm\sqrt{\epsilon}$ and at $x = y = 0$. Near these fixed points, orbits evolve according to the Jacobian $J(x, y) = \nabla \mathbf{f}$, i.e.

$$\frac{d}{dt}\delta \mathbf{x}(t) = J\delta \mathbf{x}(t). \quad (5)$$

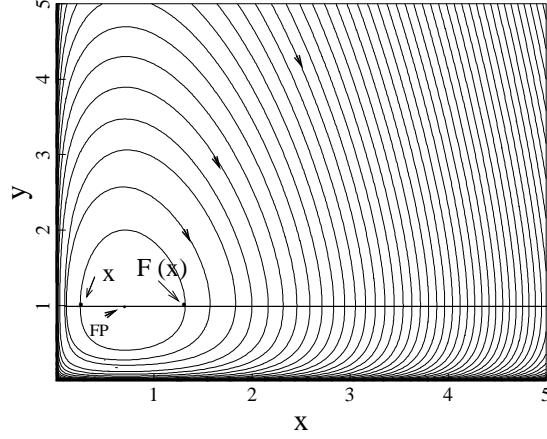


Figure 2: Contours of the Hamiltonian (3) in x, y for the Lotka-Volterra model [$\nu = 1$ in eq. (2)], showing the fixed point at $(x, y) = (\sqrt{\epsilon}, 1)$ (labeled FP) and the surface of section map $x \rightarrow F(x)$. For $\nu < 1$ the orbits spiral into the fixed point; for $1 < \nu < 2$ the orbits spiral out for all time; for $\nu > 2$ the orbits spiral out, but as soon as they cross y with a small enough value of x they go off to infinity in one pass. See Sec. 2.2.

For eqs. (1), (2),

$$J(x, y) = \begin{bmatrix} y - 1 & x \\ -2xy & \epsilon \nu y^{\nu-1} - x^2 \end{bmatrix}.$$

For the two fixed points at $x = \pm x_0, y = 1$ the eigenvalues satisfy $\lambda^2 - \epsilon(\nu - 1)\lambda + 2\epsilon = 0$, and are complex with positive real parts (unstable spirals) for

$$0 < \nu - 1 < \sqrt{8/\epsilon}. \quad (6)$$

Orbits continue to spiral out for $\nu > 1$. This is demonstrated by showing that the Hamiltonian for the case $\nu = 1$ in eq. (3) is a Lyapunov function for $\nu \neq 1$. To show this, we note

$$\frac{dH}{dt} = \frac{dx}{dt} \frac{\partial H}{\partial x} + \frac{dy}{dt} \frac{\partial H}{\partial y} = \epsilon(y - 1)(y^{\nu-1} - 1).$$

Thus, for $\nu > 1, dH/dt > 0$ and the orbits spiral outward for all time, since H has a minimum at $x = x_0, y = 1$. For $\nu < 1, dH/dt < 0$ and the orbits spiral in to the fixed point.

The system has another fixed point, but with non-analytic behavior in y for noninteger ν , at

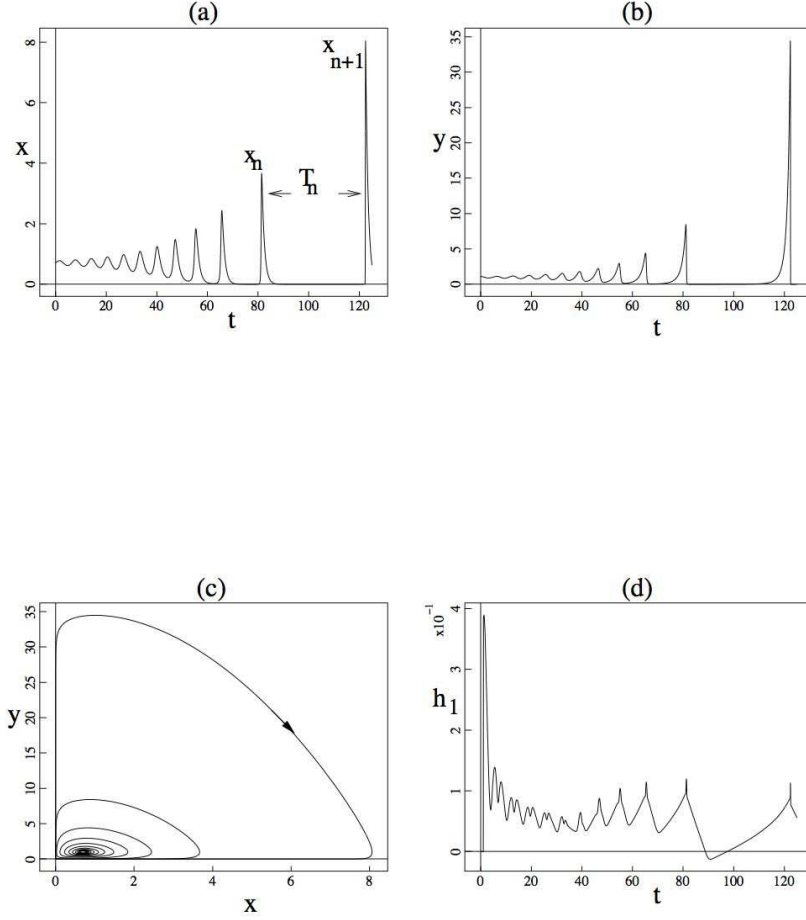


Figure 3: Orbits (a) $x(t)$, (b) $y(t)$ and (c) phase plane $y(x)$ for the deterministic equations (1) and (2), with $\epsilon = 0.5$, $\nu = 1.2$, with an initial condition near the fixed point at $x = \sqrt{\epsilon}$, $y = 1$. The orbit spirals out of the fixed point, continuing to expand, eventually piling up near the invariant manifolds $x = 0$, $y = 0$, with bursts to large values of x and y and long interburst time intervals spent mostly near $x = y = 0$. In (d) the finite time Lyapunov exponent $h_1(t)$ is shown.

$x = 0$, $y = 0$. The axes $x = 0$, $y = 0$ are invariant manifolds; we consider only $y > 0$, and for the noise-free case orbits with $x(0) > 0$ remain in that quadrant. In the range of ϵ and ν given in eq. (6), orbits spiral away from the fixed points at $(\pm x_0, 1)$ [Fig. 1], approaching the x - and y -axes, as shown in Fig. 3, which has $\epsilon = 0.5$, $\nu = 1.2$. After an initial transient, the motion is bursty, with each successive oscillation coming closer to the axes, leading to a larger interburst interval, followed by a larger burst.

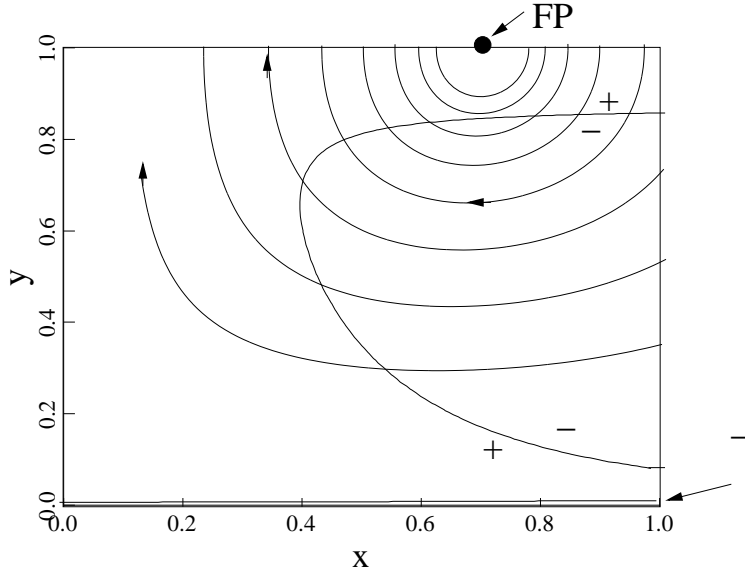


Figure 4: Zero contours of the larger eigenvalue ρ of the symmetrized Jacobian $J_s = (J + J^T)/2$, showing the fixed point (FP) $(x, y) = (\sqrt{\epsilon}, 1)$, the region (+) where $\rho > 0$ and two regions (-) where $\rho < 0$, one a very thin sliver near the x -axis. Also shown is a representative orbit spiraling out from the vicinity of the fixed point. The parameters are as in Fig. 3.

We compute the finite time Lyapunov exponent

$$h_1(t) = \frac{1}{t} \ln \left(\frac{|\delta \mathbf{x}(t)|}{|\delta \mathbf{x}(0)|} \right), \quad (7)$$

where $\delta \mathbf{x}(t)$ is evolved according to eq. (5) and $\mathbf{x}(t)$ is evolved by eqs. (2), (1). In deterministic systems with a chaotic attractor, $h_1(t)$ measures the average exponential rate of divergence, or stretching, over $0 < t' < t$. The largest Lyapunov exponent is the limit of $h_1(t)$ as $t \rightarrow \infty$ or the average, with suitable invariant measure, of $h_1(t)$ over the attractor. In this 2D system without time dependence and with diverging orbits, the infinite time Lyapunov exponent does not, strictly speaking, have significance. However, we will discuss h_1 in more detail in this section and Sec. 4.5, where the orbits are bounded and it is therefore appropriate. The exponent $h_1(t)$ is shown as a function of time in Fig. 3d. It is clear that $h_1(t)$ shows the bursts in x and y , and decreases whenever the orbit is near enough to the origin. In Fig. 4 we show the zero contours of the larger eigenvalue $\rho(x, y)$ of the symmetrized Jacobian $J_s = (J + J^T)/2$, computed analytically. This

quantity is relevant because $|\delta\mathbf{x}(t)| = (\delta\mathbf{x}(t), \delta\mathbf{x}(t))^{1/2}$ evolves according to

$$(d/dt)(\delta\mathbf{x}(t), \delta\mathbf{x}(t)) = (\delta\mathbf{x}(t), 2J_s\delta\mathbf{x}(t)) \leq 2\rho(t),$$

so that $\rho(t) = \rho(x(t), y(t))$ is an upper bound for the local contribution to $h_1(t)$, namely $(d/dt) \ln |\delta\mathbf{x}(t)| = |\delta\mathbf{x}(t)|^{-1}(d/dt)|\delta\mathbf{x}(t)| \leq \rho(t)$. From this we find $dh_1(t)/dt \leq [\rho(t) - h_1(t)]/t$, $(d/dt)(th_1) \leq \rho(t)$ or $h_1(t) \leq t^{-1} \int_0^t \rho(s)ds$.

Further insight into the bursty nature can be obtained by finding the surface of section, shown in Fig. 5 and discussed above for the Hamiltonian case $\nu = 1$. For the parameters of Fig. 3, this map $x \rightarrow x' = F(x)$ is shown in Fig. 5a. The slope $F'(x)$ at the fixed point $x = \sqrt{\epsilon}$, computed numerically, equals $s_1 = -1.17$. This value agrees with the value obtained from the complex eigenvalues λ of $J(x_0, y_0)$, which satisfy $\lambda = \lambda_r \pm i\lambda_i$ with $\lambda_r = \epsilon(\nu - 1)/2$ and $\lambda_i = \pm\sqrt{2\epsilon}(1 + O(\epsilon(\nu - 1)^2))$, which equals ± 1 for $\epsilon = 0.5$ and $\nu \ll 1$. This gives $s_1 \approx -e^{\epsilon(\nu-1)\pi/2}$. For $\epsilon = 1/2$, $\nu = 1.2$, this gives $s_1 = -1.17$, in agreement with the numerical results. This value s_1 is less than -1 , as it must be because the fixed point is unstable. Note that the values of x' for small x rise rapidly as $x \rightarrow 0$ [x' is approximately proportional to $\sqrt{-\ln x}$, as suggested by the $\nu = 1$ (Lotka-Volterra) results discussed after eq. (4)], indicating that orbits that are near $x = 0$ when they pass $y = 1$ lead to large succeeding maxima. Even more pronounced is that for $x > 3$ the values of x' are vanishingly small, showing that moderately large maxima lead to succeeding minima that are extremely close to the y -axis. In Fig. 5b we show the composite surface of section $x \rightarrow x''$, from one minimum to the next, or one maximum to the next. The slope at the fixed point is $1.37 \approx s_1^2$, as expected. For large x , $x'' = F^2(x)$ appears to be exponential in x .

Next, we turn to a discussion of the choice of the parameter ν . Let us investigate the range of the parameters ν, ϵ for which the system exhibits successively larger, more widely separated bursts.

Consider eqs. (1), (2) for large y and small x , i.e.

$$\frac{dx}{dt} = yx, \tag{8}$$

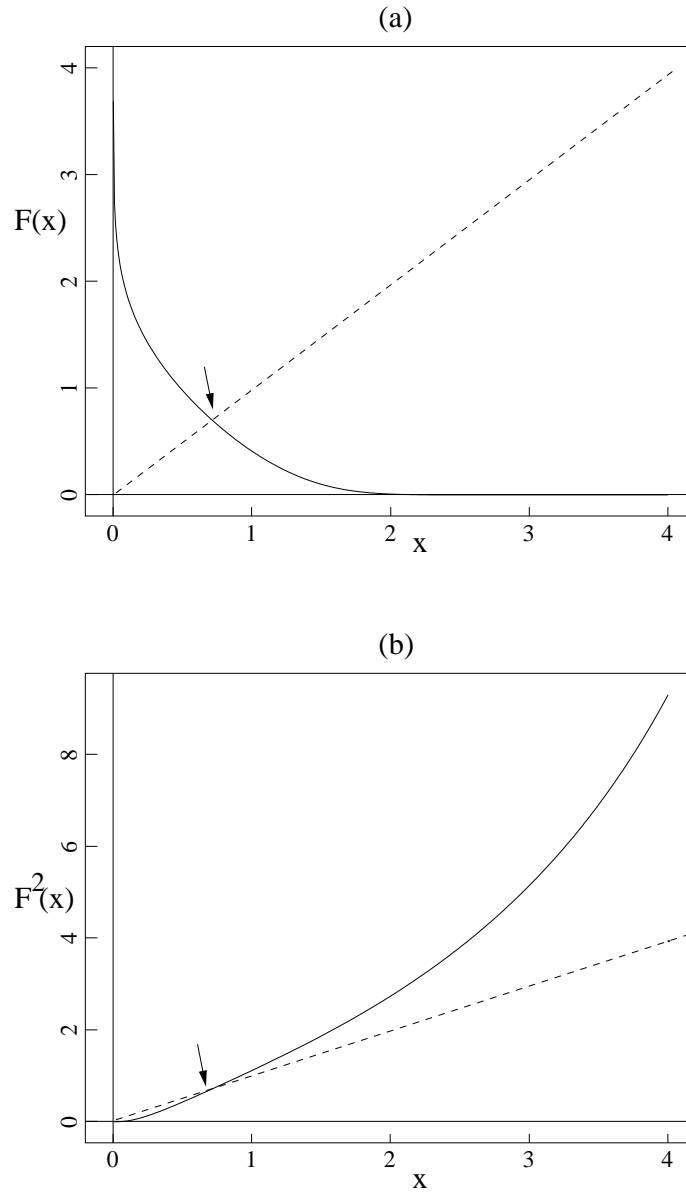


Figure 5: Surface of section (a) $x \rightarrow x' = F(x)$ from one crossing of $y = 1$ ($\dot{x} = 0$) to the next, showing $x = \sqrt{\epsilon}$ as the fixed point. Parameters are as in Fig. 3. Composed surface of section (b) $x \rightarrow x'' = F^2(x) = F(F(x))$. The dashed lines are, respectively, $x' = x$ and $x'' = x$.

$$\frac{dy}{dt} = g(0, y) \approx \epsilon y^\nu. \quad (9)$$

From these we conclude

$$x = x_c \exp \left[\frac{y^{2-\nu}}{\epsilon(2-\nu)} \right], \quad (10)$$

where $x_c \exp [1/\epsilon(2-\nu)]$ is the value of x when the orbit passes $y = 1$ with small x . Let us compare the two terms on the right in eq. (2), first for $\nu = 1$ (Lotka-Volterra). The second term exceeds the first if $x^2 > \epsilon$ and, since $x \sim e^{y/\epsilon}$, the nullcline $dy/dt = 0$ is crossed, and y eventually decreases. For $1 < \nu < 2$, the nullcline is crossed when $x^2 \geq \epsilon y^{\nu-1}$ or

$$x_c^2 \exp \left[\frac{2y^{2-\nu}}{\epsilon(2-\nu)} \right] \geq \epsilon y^{\nu-1}, \quad (11)$$

which occurs eventually. So, in each burst, y reaches a maximum and begins to decrease, starting a new cycle, as long as $x \neq 0$. (The orbits with $x = 0$ go to infinity in finite time for $\nu > 1$.)

For $\nu = 2$, we can use eq. (8) with eq. (2) for arbitrary x (including the term $-x^2y$) to obtain, for large y ,

$$\frac{dy}{dx} = \epsilon \frac{y}{x} - x.$$

The solution is

$$y = \zeta x^\epsilon - \frac{x^2}{2-\epsilon},$$

with $\zeta > 0$; the nullcline has $y = x^2/\epsilon$. For $\epsilon < 2$, the nullcline is crossed and the cycle begins again. For $\epsilon > 2$ the nullcline is not crossed and the orbit can go off to infinity in one cycle, in finite time.

For $\nu > 2$, the nullcline in eq. (11) is never reached if x_c is small enough. This means that if the value of x when the orbit crosses $y = 1$ is below some critical value, the orbit will go off to infinity before another cycle. Therefore, an orbit starting near the fixed point $(x, y) = (\sqrt{\epsilon}, 1)$ will encircle the fixed point a finite number of times and then go off to infinity in finite time.

3 Stochastic model and results

3.1 Model

With noise, the system based on eqs. (1), (2) is a nonlinear stochastic ODE, of the form

$$\frac{dx}{dt} = f(x, y) + \sqrt{2D}\xi(t), \quad (12)$$

$$\frac{dy}{dt} = g(x, y), \quad (13)$$

with $\xi(t)$ representing uncorrelated unit variance Gaussian noise, having $\langle \xi(t) \rangle = 0$, $\langle \xi(t)\xi(t') \rangle = \delta(t - t')$. Here, D is the Brownian diffusion coefficient. For a low noise level, $\xi(t)$ affects the dynamics only near the y -axis, where $f(x, y)$ is small. The motivation for including noise in the x -equation but not in the y -equation is the following. Without noise, when the orbit is traveling along the y -axis for $y < 1$, $x(t)$ can decrease to a level that is unrealistically small for modeling any physical application with noise. Noise prevents x from becoming so small for $0 < y < 1$, and therefore is expected to prevent the successive bursts from continuing to increase in magnitude, with increasing interburst time interval. We do not include noise in the y -equation because noise could cause y to become negative when the orbit is near the x -axis. We will discuss a model allowing negative y in Sec. 4.

We integrate the nonlinear stochastic ODE system (12), (13) numerically, with a noise term in x added at each time step. Specifically, the time stepping from t to $t + h$ is

$$\begin{aligned} x(t+h) &= x(t) + hf\left(\frac{x(t)+x(t+h)}{2}, \frac{y(t)+y(t+h)}{2}\right) + \sqrt{2Dh}\xi(t), \\ y(t+h) &= y(t) + hg\left(\frac{x(t)+x(t+h)}{2}, \frac{y(t)+y(t+h)}{2}\right). \end{aligned} \quad (14)$$

The implicit form of the deterministic part of the equations is solved by a simple Picard iteration. The random term is added after this iteration on the deterministic equations has converged. Each value $\xi(t)$ is an independent random number with zero mean Gaussian distribution and unit

variance, and the coefficient $\sqrt{2Dh}$ is chosen to give results independent of the time step h (in a mean-square sense) in the limit $h \rightarrow 0$.

3.2 Numerical results

Results for the same parameters as in Fig. 3, with noise having $D = 5 \times 10^{-9}$, are shown in Fig. 6, with $0 \leq t \leq 1000$. The orbits are still of a bursty nature, but the bursts and the interburst time intervals are limited in magnitude. The successive bursts appear to be uncorrelated and bursts with x negative are as common as those with x positive, after the transient near the fixed point at $x = x_0 = \sqrt{\epsilon}, y = 1$. To the eye, these results appear similar to those of a chaotic deterministic system, e.g. the $y - z$ projection of the Lorenz system[13].

In Figure 7 we show the finite time Lyapunov exponent $h_1(t)$ for the case of Fig. 6 for $0 \leq t \leq 10^4$. The orbits $\mathbf{x}(t) = (x(t), y(t))$ given by eqs. (12), (13) are affected by the noise $\xi(t)$ but the variational form for $\delta\mathbf{x}(t)$ is eq. (5) and does not directly involve the noise. [Two orbits $\mathbf{x}_1(t)$ and $\mathbf{x}_2(t) = \mathbf{x}_1(t) + \delta\mathbf{x}(t)$ with slightly different initial conditions are integrated in time with the same realization of the noise $\xi(t)$.] For these parameters $h_1(t)$ converges to 0.032 as $t \rightarrow \infty$. For several other values of ϵ, ν , and D , with $1 < \nu < 2$ and (6), similar results are obtained. This positive Lyapunov exponent shows exponential divergence between nearby orbits. This suggests what appears to be evident from Fig. 6, namely that the orbits behave chaotically. This conclusion is reasonable because the system with noise is 2D with time dependence, and because the orbits remain bounded for the time intervals studied, during which $h_1(t)$ appears to converge to a constant value. We will return to this discussion in Sec. 4.5.

To analyze the bursts in terms of amplitude and time interval between bursts, we introduce x_n, x_{n+1} and T_n . (See Fig. 3.) These are, respectively, the amplitude (in x) of a burst (a local maximum for positive x , a local minimum for negative x), the amplitude of the following burst, and the time interval between them. In Fig. 8 we show scatter plots of T_n vs. x_n, x_{n+1} vs. T_n , and the composite x_{n+1} vs. x_n for the parameters of the case of Figs. 6 and 7, indicating the probability density functions $f_1(x_n, T_n), f_2(T_n, x_{n+1})$ and $f_3(x_n, x_{n+1})$. These are the marginal distributions

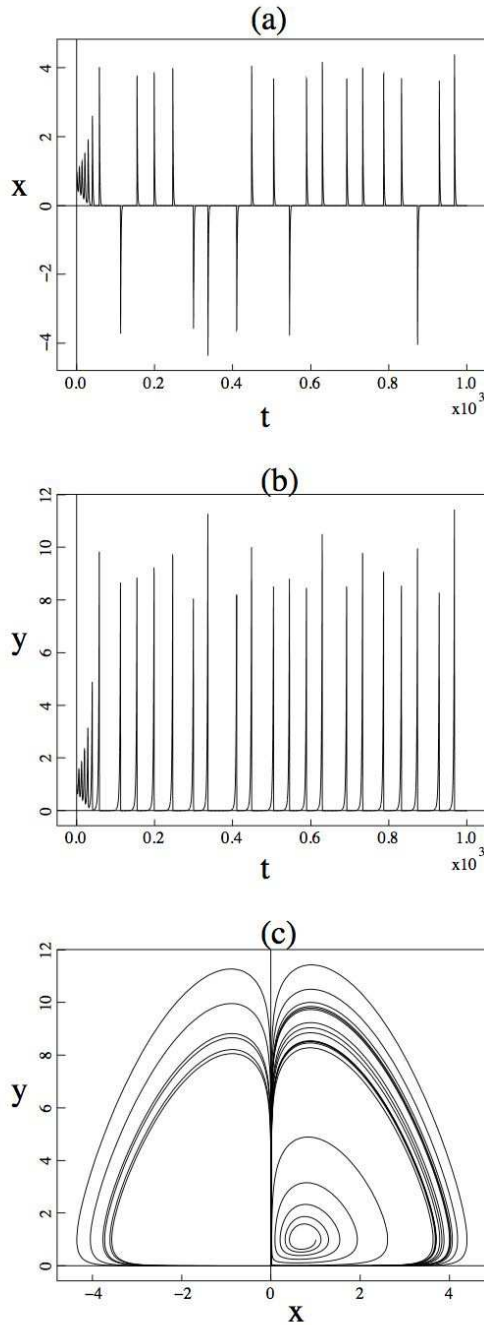


Figure 6: Orbits (a) $x(t)$, (b) $y(t)$ and (c) phase plane y vs. x for the system with noise, eqs. (12) and (13). The parameters are equal to those in Fig. 3, with $D = 5 \times 10^{-9}$. The initial condition is near the spiraling fixed point, so that the transient spiral shows. Note that the maximum time $t = 10^3$ is much larger than in Fig. 3.

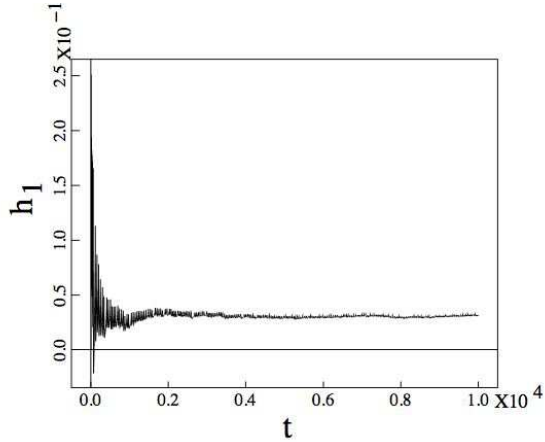


Figure 7: The finite time Lyapunov exponent up to $t = 10^4$, for the case of Fig. 6, showing a positive limiting value, $\lim_{t \rightarrow \infty} h_1(t) = 0.032$.

of the full distribution $g(x_n, T_n, x_{n+1})$ projected over x_{n+1} , x_n , and T_n , respectively. The first has very little scatter. This property is related to two aspects. One is the fact that the noise is added only to $x(t)$ and has little effect except when x is small. The other is that most of the time interval T_n is spent near the saddle at $x = y = 0$, after the burst but before the orbit can be influenced again by the noise, as it passes along the y -axis near $y = 1$. This lack of scatter shows a very strong correlation. However, this correlation is strongly nonlinear and would not be reflected in the linear correlation coefficient, but would require a diagnostic such as the conditional entropy [14]. The other plots show the expected symmetry in x . Specifically, there are four equivalent peaks in the four quadrants in Fig. 8c, showing that successive peaks are positive or negative, independent of the sign of the previous peak. Fig. 8b shows a long tail in T_n , and sharp cutoffs for small $|x_n|$ and small T_n .

In Fig. 9 are histograms, showing the marginal distributions of x_n , at the maxima of $|x|$, and the interburst time T_n . (See Fig. 3.) The maximum time was $t = 10^6$ and there were about 23000 peaks in x_n and the same number of interburst intervals T_n . The histogram of x_n is symmetric and shows peaks at $|x_n| = 3.7$, with tails around $|x_n| = 4.5$ and a sharp cutoff inside at $|x_n| = 3.3$. The latter histogram, reflecting the nonlinear correlation of T_n with x_n shown in Fig. 8a, has a strong

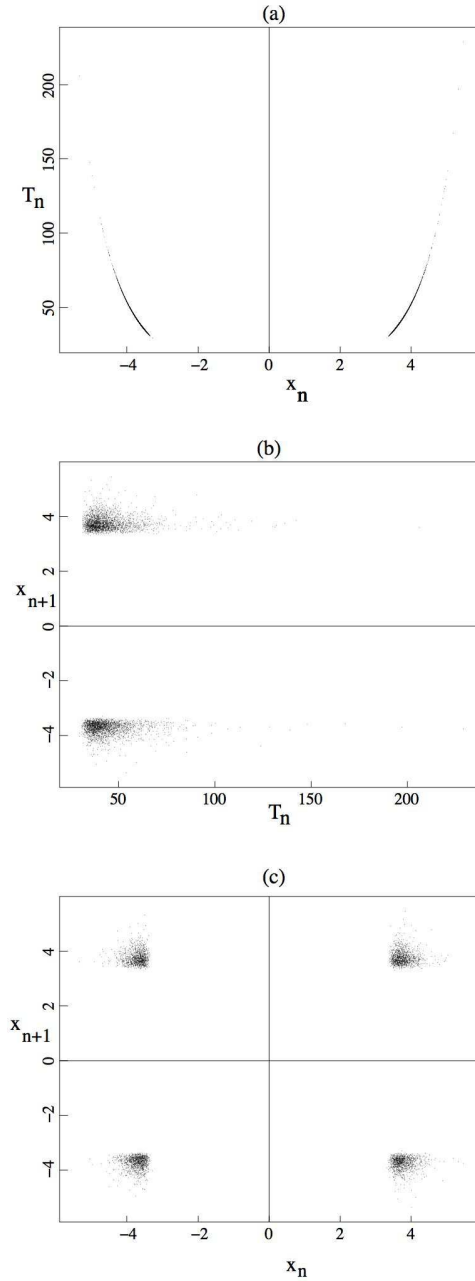


Figure 8: Scatter plots (a) T_n vs. x_n , (b) x_{n+1} vs. T_n and (c) x_{n+1} vs. x_n for the case of Fig. 6. Note that there is hardly any scatter in (a). The extent of the burst [measured as $|x_n|$ or as the peak of $y(t)$] determines T_n , because after a larger burst the orbit approaches the origin closer to the x -axis, because most of the interburst time is spent near $x = y = 0$, and because the noise is effective only near the y -axis. The statistics plotted in (b) is symmetric in x_{n+1} and has a long tail in T_n . The plot in (c) is symmetric in x_n and x_{n+1} , with four essentially identical peaks near $|x_n| = |x_{n+1}| = 4$.

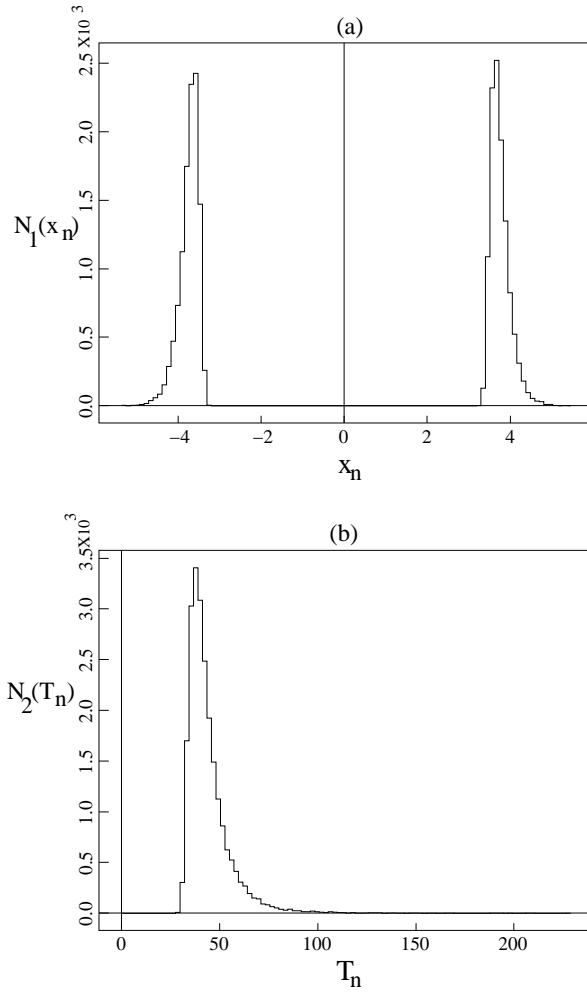


Figure 9: Histograms $N_1(x_n)$, $N_2(T_n)$ of (a) x_n , maxima of $|x|$ and (b) time intervals T_n , respectively, showing the marginal distributions for these quantities. The histogram of $|x_n|$ in (a) has tail with $|x_n| \gtrsim 5$ and a strong cutoff for $|x_n| < 3.3$; T_n in (b) also has a tail to the right and a sharp cutoff to the left. For this case the mean values are $\langle |x_n| \rangle = 3.87$ and $\langle T_n \rangle = 49.1$, respectively.

cutoff inside $T_n = 30$, a peak at $T_n = 38$, and a tail for $T \sim 60 - 80$.

Based on Sec. 2.2, we expect considerably different results for $\nu > 2$. These results show that, for the deterministic system, if the value of x at the *throat* $y = 1$ is small enough, the orbit will go off to infinity before another cycle occurs. Therefore, we expect that if the noise level D is small enough, the orbit may have a few bursts, but will diverge to infinity as soon as the cycle comes close enough to $x = 0$ as it crosses $y = 1$. For large values of D , the orbit may behave as in Fig. 6 for a very long time, but whenever x becomes small enough at the inner crossing of $y = 1$, the orbit will also go to infinity before another cycle. Numerical simulations bear this out.

3.3 Fokker-Planck analysis near $x = 0$

The peaks discussed in Figs. 8 and 9 are maxima in $|x|$, which occur at $y = 1$. These are related to the values of x near zero for which $y = 1$: for small values of D , the noise is important only near the y -axis, and as the orbit lifts off this manifold it essentially obeys the deterministic equations, and therefore the peaks in $|x|$ are determined to high accuracy by the crossing of $y = 1$ for small x . In this section we quantify this behavior by means of analysis involving the Fokker-Planck equation for behavior near the y -axis.

As the orbit travels near the y -axis, $x(t)$ satisfies the linear stochastic equation

$$\frac{dx}{dt} = \gamma(t)x + \xi(t), \quad (15)$$

where $\gamma(t) = y(t) - 1$; for small x , y satisfies $\dot{y} = \epsilon y^\nu$, independent of x . The noise $\xi(t)$ has the statistical characteristics described after eqs. (12), (13). Linearization in x holds for small D , up to the time when the term $-x^2 y$ in eq. (2) becomes important. For low noise level (small D), the successive bursts are large in magnitude, leading to small values of x on the next pass. On each successive pass near $y = 1$, the correlation with the previous peak of $|x|$ is lost, according to the results shown in Fig. 8. This behavior is due to the fact that for $g(0, y) = \epsilon y^\nu$ with $\nu > 1$, x becomes small enough to become dominated by the noise while $y < 1$.

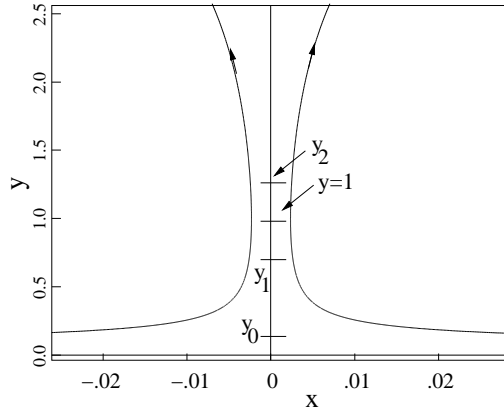


Figure 10: Sketch of deterministic orbits near $x = 0$. The minima of $|x|$ are at the throat $y = 1$. In this region, the equations can be linearized with respect to x and noise can have a large influence. The values $y = y_1, 1, y_2$ correspond to $t = t_1, 0, t_2$ in the text.

In Appendix A we have included an analysis based on the Fokker-Planck equation for orbits near $x = 0$, where eq. (15) is valid. Conclusions based on this Fokker-Planck analysis and direct simulations are the following. The mean value $\langle |x_n| \rangle$ (c.f. Fig. 9a) decreases with D . The dependence of this quantity is shown as a function of D in Fig. 11a. The mean of the histogram of the interburst time T_n as a function of D is shown in Fig. 11b. The results for small D in Fig. 11a are qualitatively similar to the behavior of $F(x)$ shown in Fig. 5a. This is expected because, as we have discussed in Appendix A, the orbits cross $y = 1$ with typical values of x proportional to $\sigma_x \sim \alpha^{1/2} \sim D^{1/2}/\epsilon^{1/4}$, and proceed with little subsequent effect of noise. The dependence of $\langle |x_n| \rangle$ on D appears to be approximately logarithmic for small D , consistent with the approximately logarithmic behavior of the map F shown in Fig. 5a. It is also interesting to note that, although h_1 increases with D , the increase is logarithmic (for $D \lesssim 5 \times 10^{-5}$) and slow, varying by just over a factor of two for $5 \times 10^{-12} < D < 5 \times 10^{-4}$. This logarithmic behavior extrapolates to $h_1 = 0$ at the very low level $D = 10^{-19}$, giving $\sqrt{2Dh} = 2 \times 10^{-11}$ [c.f. eq. (14)]. Near this value of D , h_1 appears to begin to diverge from logarithmic behavior to remain positive. However, at these low noise values, roundoff is comparable to the applied noise.

The analysis in Appendix A shows that for small x , near the intersection with $y = 1$, x has a Gaussian distribution, $f(x) \propto e^{-x^2/2\sigma_x^2}$. This yields a distribution for x' , at the next crossing of

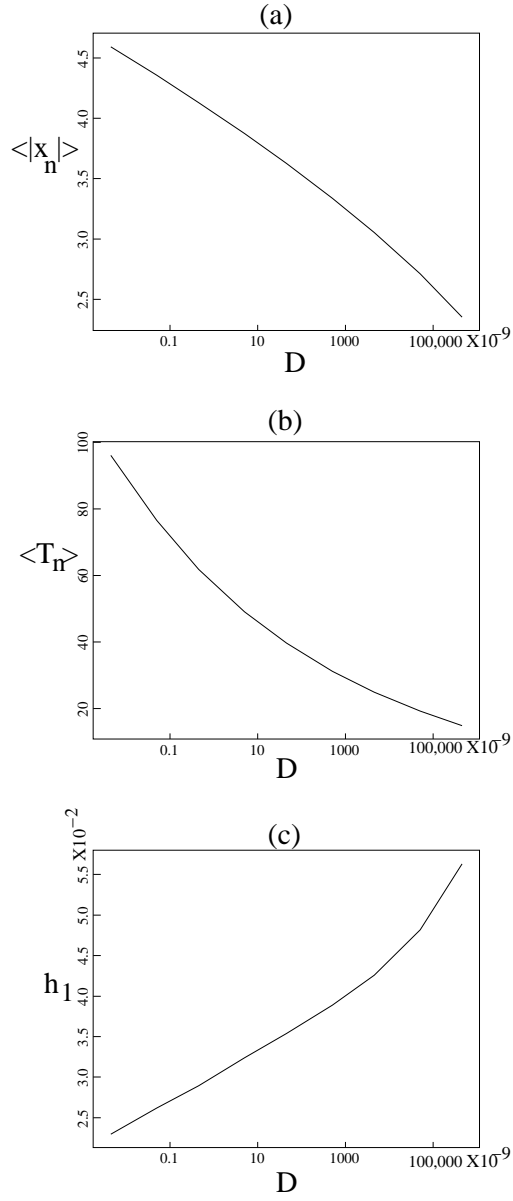


Figure 11: Mean values of (a) the burst peaks $\langle |x_n| \rangle$, (b) the interburst time $\langle T_n \rangle$ and (c) the Lyapunov exponent h_1 as functions of D . The parameters (except for noise level) are the same as in Fig. 6. The quantities $\langle |x_n| \rangle$ and h_1 appear to behave logarithmically for small D .

$y = 1$ where $|x_n|$ is a maximum, equal to

$$g(x') = |dx/dx'|f(x(x')),$$

where the functional form for $x(x')$ is shown in Fig. 5a. The second factor is responsible for the sharp cutoff to the left of the peak in x' (Fig. 9a), corresponding to x being in the tail of the Gaussian. The tail to the right of the peak in Fig. 9a is due to the Jacobian factor $|dx/dx'|$. For example, for $\nu = 1.2$ the behavior for small x from Fig. 5 is similar to that for $\nu = 1$, derived after eq. (4), namely $x' \sim \sqrt{-\ln x}$. From the Gaussian form for $f(x)$ we obtain $|dx/dx'| \sim x'e^{-x'^2}$ and

$$g(x') \propto \left(x'e^{-x'^2}\right) e^{-\frac{x(x')^2}{2\sigma_x^2}}.$$

The first (Jacobian) factor $x'e^{-x'^2}$ gives a Gaussian-like tail for large x' and the second factor gives a cutoff for x' close to the fixed point $x' = x_0 = \sqrt{\epsilon}$, where $x' - x_0 = -s_1(x - x_0)$. This cutoff is sharp if $\sigma_x \ll x_0$.

4 The role of symmetry and relation with other models

We have commented that the system (12), (13) has certain features that are not generic. These issues are (a) the reflection symmetry of the equations in x ; (b) the fact that deterministic orbits eventually go to infinity, and (c) the non-analytic behavior of y' near $y = 0$. In this section we discuss results obtained when the system is modified in these areas. To deal with issue (a), we destroy the symmetry in x by an offset [a constant term added to eq. (12)]. These results suggest a modification to the notion of structural stability in the presence of noise: the behavior is qualitatively unchanged if the offset is small relative to the noise. To deal with issue (b), we show results in which the behavior for large y is modified, preventing orbits from going to large y . Regarding issue (c), we modify the system near $y = 0$ to remove the non-analytic behavior there. We also discuss modifications breaking the reflection symmetry in x together with limiting the

behavior for large y . Finally, we discuss modifications to the system involving adding a sinusoidal perturbation to eq. (1) in place of the noise term. In these studies, conventional deterministic chaos, characterized by a Lyapunov exponent, is observed and compared with results with noise.

4.1 Breaking of the symmetry in x

We have investigated the effect of breaking the reflection symmetry $x \rightarrow -x$ in eqs. (12), (13), motivated by the experimental results shown in Sec. 5.3. The simplest way of breaking this symmetry is to introduce a constant offset. With this offset, eq. (12) takes the form

$$\frac{dx}{dt} = (y - 1)x + a + \sqrt{2D}\xi(t), \quad (16)$$

with the y -equation unchanged. Numerical results with zero noise show that for $a > 0$ a stable limit cycle is formed to the right of $x = 0$, and points near $(x, y) = (0, 0)$ go into this limit cycle. (For $a < 0$ the results are identical, with $x \rightarrow -x$.) Therefore the zero noise results of Sec. 2 are not structurally stable with respect to such an offset.

However, in the presence of noise, the results change considerably. In Figs. 12a,b we show $x(t)$ and the phase portrait y vs x for a case with the same parameters as in Fig. 6 (in particular with $D = 5 \times 10^{-9}$), but with $a = 5 \times 10^{-5}$. The results are qualitatively similar to those in Fig. 6 except that most of the bursts go to the right. In Fig. 12c we show the fraction Φ of bursts that go to the left as a function of the offset a for three values of D , and in Fig. 12d we show the Lyapunov exponent h_1 . For $a \lesssim \sqrt{D}$, h_1 and the fraction Φ are appreciable and the orbits behave qualitatively as in Fig. 6. For $a \gtrsim \sqrt{D}$, on the other hand, virtually all the orbits go to the right ($\Phi \approx 0$) and have negative Lyapunov exponent and therefore behave qualitatively as the limit cycle found for $D = 0$, $a > 0$. These results, and those of Appendix A showing $\sigma_x \sim \sqrt{D}$, indicate that the offset changes the results qualitatively if it moves the orbit outside the region near $x = 0$ where noise dominates.

This brings up the issue of structural stability of the behavior observed for $a = 0$. For zero

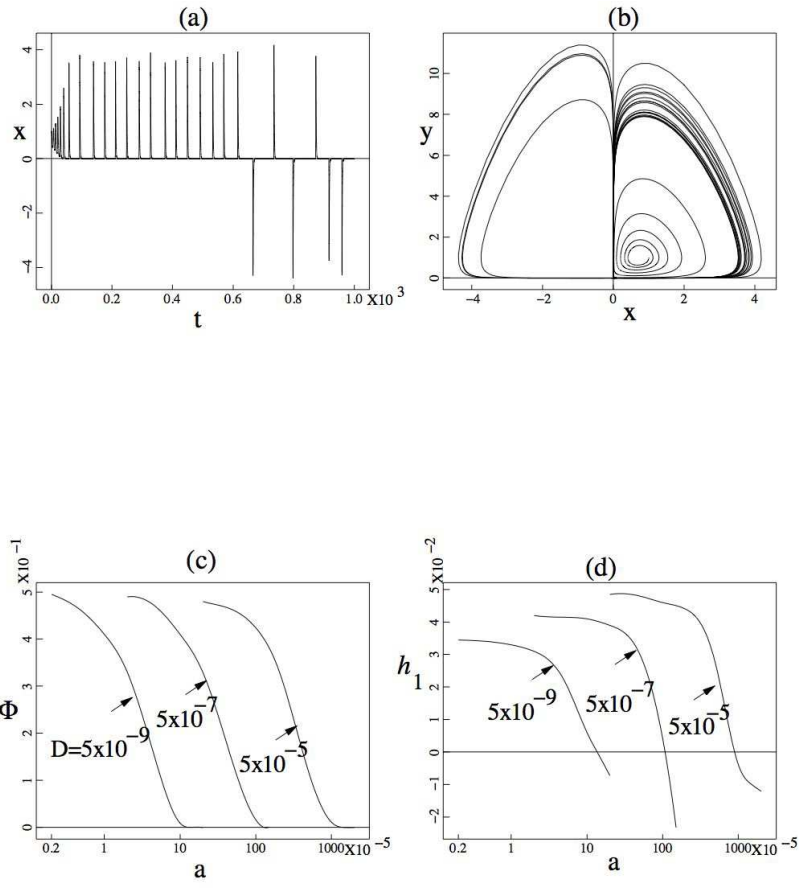


Figure 12: Results with an offset [c.f. a in eq. (16)]. In (a), (b) are $x(t)$ and y vs x for parameters as in Fig. 6, again with $D = 5 \times 10^{-9}$. In (c), (d) are the fraction Φ of bursts to the left and the Lyapunov exponent h_1 , for three values $D = 5 \times 10^{-9}, 5 \times 10^{-7}, 5 \times 10^{-5}$.

noise, this behavior, seen in Fig. 3, is certainly not structurally stable. However, for $D > 0$ the qualitative behavior persists as long as $a \lesssim \sqrt{D}$. In this modified sense, the system with finite noise is structurally stable.

We will return to the issue of an offset in the electronic circuit in the next section.

4.2 Modifications for large y

We have discussed the deterministic model for $\nu > 2$ in Sec. 2, showing that orbits go to infinity after a few passes near the fixed point $(x, y) = (x_0 = \sqrt{\epsilon}, 1)$. The dynamics in the presence of noise is the following: if the noise is large enough, the value of x at the throat where $y = 1$ will typically be large enough that the system encircles $(x_0, 1)$ many times. Even with noise, however, eventually an orbit comes through the throat with small enough x for the system to go to infinity before another cycle can occur.

A system related to eqs. (1), (2) with orbits that do not go to infinity is the predator-prey system of Odell [15, 12]. This system can be put into the form

$$\frac{dX}{ds} = X(Y - \eta),$$

$$\frac{dY}{ds} = Y^2(1 - Y) - XY,$$

or by a change of variables ($X = \eta x^2/2$, $Y = \eta y$, $s = 2t/\eta$)

$$\frac{dx}{dt} = (y - 1)x, \tag{17}$$

$$\frac{dy}{dt} = \epsilon y^\nu (1 - \eta y) - x^2 y, \tag{18}$$

with $\epsilon = \nu = 2$, i.e. the form of eqs. (1), (2) with $\nu = 2$ and $y^2 \rightarrow y^2(1 - \eta y)$. This system has fixed points at $x = \pm\sqrt{\epsilon(1 - \eta)}$, $y = 1$. For $\epsilon = \nu = 2$ these fixed points are unstable if $\eta < 1/2$ and oscillating (complex eigenvalues) if $\eta < \sqrt{3}/2$. This system also has a saddle at

$x = y = 0$, with zero eigenvalue in the y direction. In addition, it has a fourth fixed point, with $x = 0$ and $y = 1/\eta$. This fixed point is a saddle, stable in the y -direction and unstable in the x -direction; the section of the y -axis with $0 < y < 1/\eta$ is a heteroclinic line. Because of the presence of this saddle, there are two stable limit cycles, related by the reflection symmetry in x , to which typical orbits converge. For η small, this limit cycle has large excursions, with peaks in y approaching $1/\eta$. We have studied eqs. (17), (18) with noise in x , and with ϵ, ν in the range of parameters of Fig. 3. The results are similar to those of (12), (13), as long as D is large enough that the excursions almost always have $y \ll 1/\eta$. Specifically, the value of h_1 and the probability density plots as in Figs. 8, 9 are essentially identical. The effect of positive η is similar to the effect of clipping the voltage corresponding to y in the circuit (see Appendix B), except that by design the clipping turns on much more rapidly than the factor $(1 - \eta y)$ in eq. (18).

4.3 Modifications near $y = 0$

We have studied the system (12), (13) with $\epsilon y^\nu \rightarrow g_0(y) = \epsilon(\beta y + y^\nu)$. This modification regularizes the vicinity of $y = 0$: the saddle at the origin is no longer dominated by y^ν , and has eigenvalues $-1, \epsilon\beta$. The spiraling fixed points have $x = \pm x_0 = \pm\sqrt{\epsilon(1 + \beta)}$, $y = 1$. We have found that noise has the same qualitative influence for positive β as it does for $\beta = 0$. In Fig. 13a we show the scatter plot $x_n \rightarrow x_{n+1}$ for $D = 5 \times 10^{-5}$, $\epsilon = 1.5$, $\nu = 1.2$, and $\beta = 0, \beta = 1$ superimposed. For $\beta = 1$ the eigenvalue $\epsilon\beta > 1$, which implies that, when following a deterministic orbit along the x -axis and up along the y -axis, it ends up further from the y -axis than it started from the x -axis. (For the equations linearized about the origin, $x^{\epsilon\beta}y$ is constant.) This is related to the liftoff phenomenon of Refs.[7, 8]. Based on this consideration, one might expect that the sign of x_{n+1} might correlate with the sign of x_n , and the symmetry of the scatter plot would be broken, with the distribution $f_3(x_n, x_{n+1})$ having more points in the NE and SW quadrants and fewer in the SE and NW quadrants, while of course still preserving the symmetry in the marginal distribution of x_n , $\int f_3(x_n, x_{n+1})dx_{n+1}$. Nevertheless, the scatter plot for $\beta = 1$ appears to have the same symmetry as for $\beta = 0$.

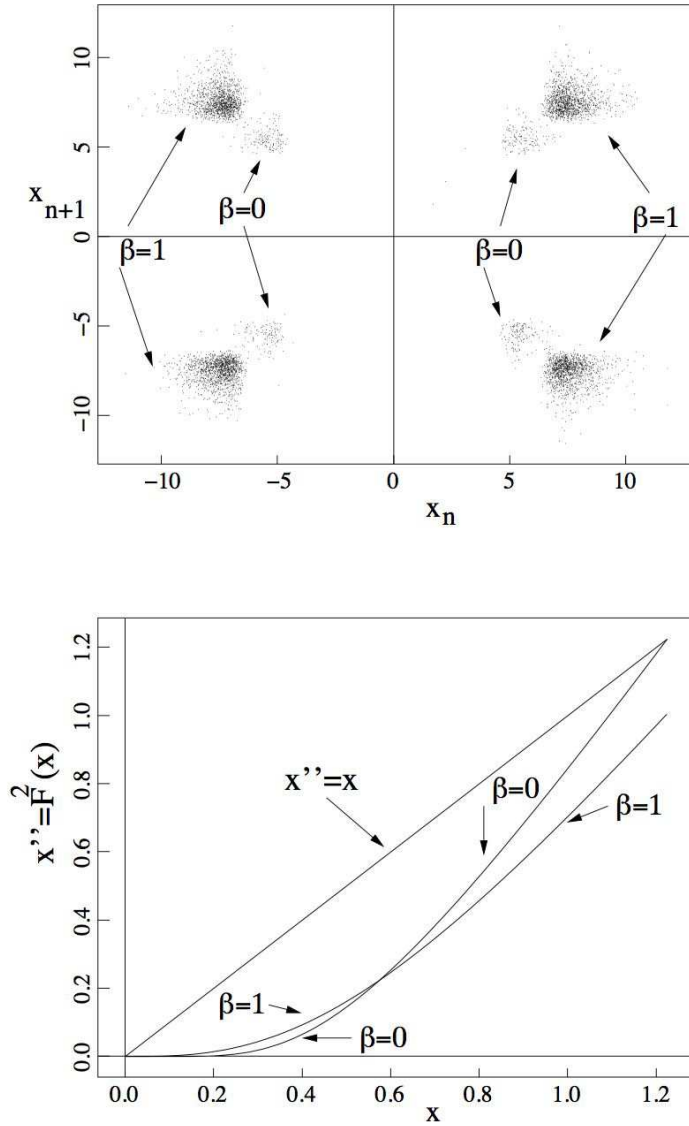


Figure 13: Scatter plot (a) $x_n \rightarrow x_{n+1}$ in the notation of Fig. 3 (successive maxima of $|x|$), for $\epsilon = 1.5$, $\nu = 1.2$, $D = 5 \times 10^{-5}$ and both $\beta = 0$ and $\beta = 1$, showing four-fold symmetry in both cases. Surface of section $x \rightarrow x'' = F^2(x_n)$ (b) for $0 < x < \sqrt{\epsilon(1 + \beta)} = 1.22$ for the deterministic case with $\epsilon = 1.5$ and both values of β . For $\beta = 1$ the fixed point is at $x = \sqrt{\epsilon(1 + \beta)} = 1.73$.

This four-fold symmetry is explained by Fig. 13b, which shows the surface of section $x \rightarrow x'' = F^2(x)$ for $0 < x < x_0$, similar to that in Fig. 5b. For both cases $x'' \ll x$. For these parameters $x'' \sim x^3$ for $\beta = 1$, while x'' goes to zero faster than any power when $\beta = 0$. The origin is so very attracting for F^2 because small x maps to large x' under F and the orbit from there passes extremely close to $y = 0$, thereby leading to extremely small x'' in spite of $\epsilon\beta > 1$. Because of this property, if an orbit starts with $x \sim \sigma_x$ at $y = 1$ and executes one cycle, the value $x = x''$ when it crosses $y = 1$ after this cycle will be so small ($x'' \sim \sigma_x^3$ for $\beta = 1$) that it is dominated by the noise added for small x and will even for $\beta = 1$ be nearly independent of x . This four-fold symmetry was observed for these parameters for $5 \times 10^{-13} < D < 5 \times 10^{-3}$.

Although the increase of β has no effect on the symmetry of the scatter plot $x_n \rightarrow x_{n+1}$, it has a profound influence on the burst intervals T_n . For larger β , typical values of T_n (not shown) are much smaller because of the liftoff phenomenon. This dependence of T on β is understood easily. Suppose the orbit enters the region $[0, a] \times [0, b]$ with $y = y_0$. We find that if $\beta y \gg y^\nu$, the time to exit the region equals $T_1 \equiv (1/\epsilon\beta) \ln(b/y_0) \sim \beta^{-1}$. If, on the other hand, $\nu > 1$ and the orbit is far enough from the origin that $y^\nu \gg \beta y$, then β can be neglected and the time interval equals $T_2 \equiv (y_0^{1-\nu} - b^{1-\nu}) / [\epsilon(\nu - 1)]$. For example, for $\epsilon = 1.5, \beta = 1, \nu = 1.2, b = 1, y_0 = 10^{-4}$ we find $T_1 = 6.1$ and $T_2 = 18$.

We have considered other models in which $g_0(y)$ is linear in y near $y = 0$ but behaves as ϵy^ν for large y . The cases investigated were $g_0(y) = \epsilon y(\beta^p + y^{p(\nu-1)})^{1/p}$ for various values of p , including $p = 1$. [Note that g_0 is analytic at $y = 0$ if $p(\nu - 1)$ is an integer.] The results for all the tested values of p are similar to the $p = 1$ case described above.

We have also considered the case $g_0(y) = \epsilon(\beta y + y^2)$. In Sec. 2 we concluded that the deterministic system for $\nu = 2$ continued to have bursts of increasing amplitude and time interval (rather than being capable of going to infinity in finite time in a single burst) if $\epsilon < 2$. Results for various values of $\epsilon < 2$ and D show that the results are similar to those for $\nu < 2$, as long as ϵ is small enough, β is large enough, and D is large enough. Note that for this case the flow is analytic everywhere, including $y < 0$, and that for the deterministic form there is a fixed point

at $x = 0$, $y = -\beta$, as well as the fixed point at the origin, the latter having the x -axis as its stable manifold. This new fixed point is attracting in both directions, and therefore any noise in the y -direction eventually leads the orbit to this fixed point.

4.4 Limitation for large y with asymmetry in x

A phase portrait for a flow including both saturation in y and symmetry breaking in x [c.f. eqs. (16), (18)],

$$\begin{aligned}\frac{dx}{dt} &= (y - 1)x + a, \\ \frac{dy}{dt} &= \epsilon y^\nu (1 - \eta y) - x^2 y,\end{aligned}$$

is shown in Figure 14, with $\eta = 0.1$ and $a = 0.015$. The unstable spirals are now slightly asymmetric due to the finite value of a . There are two saddle points near the origin, at $x = a$, $y = 0$ and at $x \approx a$, $y \approx (a^2/\epsilon)^{1/(\nu-1)}$. For these parameters, the second fixed point has $y \sim a^{10}/\epsilon^5 \sim 10^{-17}$, and the dynamics of the system can be described as if only the saddle at $x = a$, $y = 0$ exists. This saddle still has the x -axis as its stable manifold (with right and left pieces labeled $1SR$ and $1SL$). The unstable manifold of this saddle (labeled $1U$) now is no longer the y -axis, but bends slightly to the right and eventually asymptotes to a limit cycle (not shown) orbiting the right spiral fixed point. Another saddle at approximately $x \sim -a\eta$, $y \sim 1/\eta$ (filled circle) has an unstable manifold with right and left pieces (labeled $2UR$ and $2UL$, respectively). The invariant manifolds bend downward, coming into the vicinity of the x -axis, pass very close to the saddle at the origin, and both converge onto the unstable manifold $1U$, thus approaching the limit cycle on the right as well. The stable manifold for the upper saddle point, labeled $2S$, if followed backward in time, asymptotes to the spiral on the left. Hence, a narrow region on the y -axis near $y = 1$ that is bounded by $2S$ on the left and $1U$ on the right sets the scale for the noise response. If the noise amplitude is smaller than the width of this region (denoted Δ), nearly all points passing through this region will go to the right and asymptote to the limit cycle. If $\sigma_x > \Delta$, then orbits will get kicked to the left and right with nearly equal probability, leading to noise stabilized behavior that

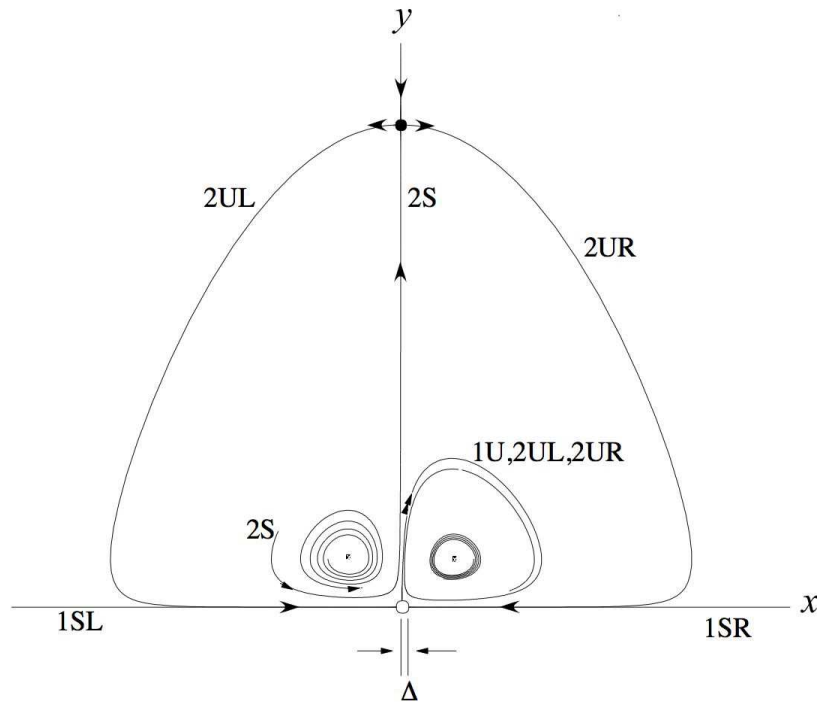


Figure 14: Phase portrait for the deterministic system of equations with limiting in y and offset in x , with zero noise and $\nu = 1.2$, $\epsilon = 0.5$, $a = 0.015$, $\eta = 0.1$. There is a saddle near the origin (open circle), a saddle near $y = 1/\eta$ (filled circle), two unstable spirals, and a stable limit cycle (not shown) on the right. The symbols $1SL$, $1SR$, and $1U$ represent the left and right arms of the stable manifold of the fixed point near the origin and its unstable manifold. The lower arm of the stable manifold of the fixed point near $y = 1/\eta$ is $2S$ and its unstable manifold is $2UL$, $2UR$. Points from the spiral on the right go to the stable limit cycle; points from the fixed point on the left eventually end up outside $2S$ and go to the same limit cycle.

prevents the relaxation onto the limit cycle.

Thus, the presence of the symmetry breaking term in the deterministic dx/dt equation destroys the heteroclinic connection between the two saddle points, leading generically to a limit cycle either on the right or left, depending upon the sign of the offset. Thus, the deterministic dynamics for $a = 0, \eta > 0$ discussed in Sec. 4.2 is not structurally stable, but the behavior with noise is structurally stable in the sense discussed at the end of Sec. 4.1. The noise response is very similar to the noise response of the model with $\eta = a = 0$ (Sec. 3), to the model with $\eta = 0, a \neq 0$ (Sec. 4.1) and to the model with $\eta > 0, a = 0$ (Sec. 4.2).

4.5 Sinusoidal perturbation

We have integrated eqs.(1), (2) with a sinusoidal term $\xi(t) = b \sin(\omega t)$ added to the x -equation rather than random noise. We chose ω to be large enough so that the sine goes through many cycles when the orbit is along the x -axis, but large enough to avoid aliasing, i.e. $\omega h < \pi$, where h is the time step. The sinusoidal and random forms of $\xi(t)$ are extremes of temporal driving, with quasiperiodic time dependence and colored random time dependence as intermediate cases. In all such cases the analysis of Sec. 3.2 indicates that the typical value of x at $y = y_2$ is the important factor. (See Sec. 3.2 and Fig. 10.) This suggests that the Lyapunov exponent h_1 has validity in all these cases. To explore this further, we have obtained results for $\nu = 1.2, \epsilon = 0.5$, as in Fig. 6, and with various values of ω and b . The results were found to be qualitatively similar to those with noise, with a simple relation between b and D , showing that indeed the accumulated effect on x at the time $y = y_2$ is the determining factor. That is, $\sigma_x \sim b/\omega$ or $b/\omega \sim D^{1/2}/\epsilon^{1/4}$. In particular, the behavior of $\langle |x_n| \rangle, \langle T_n \rangle$ and h_1 are similar. Thus, the similarity of the results with this deterministic non-autonomous system and the nonlinear stochastic system (12), (13) lend credence to the idea that h_1 as defined in Sec. 2 and used in Sec. 3.1 is the appropriate form of the Lyapunov exponent for the stochastic system. It is known that a system with periodic driving can be distinguished from an autonomous system or one with more complex temporal driving by means of nonlinear symbolic time series analysis[16]. This distinction is possible because of

definite dips in the conditional entropy of symbolic time series when the sampling time equals the period $2\pi/\omega$ [16]. This condition distinguishes periodic driving from all other temporal driving (autonomous, quasi-periodic, colored noise, white noise), but does not distinguish the other possible varieties from each other. This topic is outside the scope of the present investigation.

5 Electronic circuit

In order to test for noise stabilization in a physical system, we have constructed a circuit which integrates eqs. (13) and (14). In dimensionless integral form, these equations are $x(\tau) = x_0 + \int_{\tau_0}^{\tau} \left((y-1)x + \hat{\xi}(\tau') \right) d\tau'$ and $y(\tau) = y_0 + \int_{\tau_0}^{\tau} (\epsilon y^{\nu} - x^2 y) d\tau'$, and the parameter values used in the circuit were $\epsilon = 0.5$ and $\nu = 1.2$, as in Figs. 3,5-9,11,12. The circuit design is shown in Fig. 18. The white noise, $\hat{\xi}(t) = \sqrt{2D}\xi(t)$, stabilized the oscillations, and Figs. 15-17 show that the circuit output agreed well with numerical solution of eqs. (13) and (14). We also observed the structural instability in these equations. See Appendix B for a description of the circuit design.

5.1 Properties of the added noise

The noise was generated by creating random numbers and recording them to a `.wav` file to play back via the computer's audio output at the standard rate of 44 kHz. This net process effectively filters the noise through a lowpass filter. When we sampled the noise using a digital oscilloscope, we found that the noise had a relatively constant spectrum to frequencies as high as 20 kHz. We autocorrelated the noise, and found that it was well represented by:

$$\langle V_N(t)V_N(t') \rangle = \frac{A_0}{\pi(t-t')} \sin 2\pi \frac{(t-t')}{T}$$

with a period $T = 50 \mu\text{s}$, which also represents a flat spectrum filtered by a 20 kHz low-pass filter. For times longer than $T/(2\pi)$, this autocorrelation function is a good approximation of $A_0\delta(t)$. By evaluating the autocorrelation function at $t = 0$, we can determine that $A_0 = \frac{T}{2} \langle V_N^2 \rangle$ so the

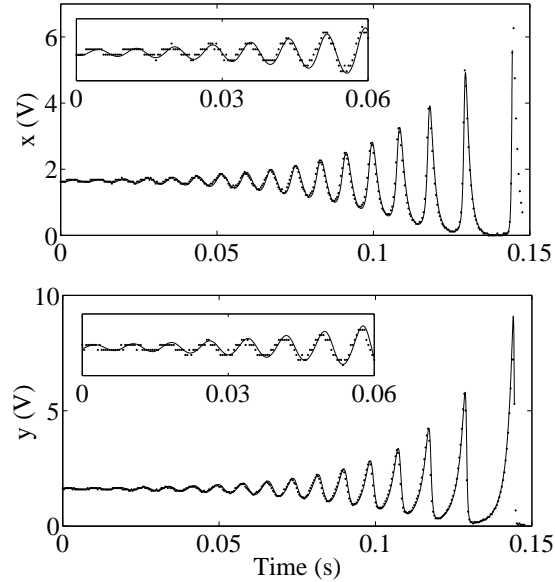


Figure 15: Circuit output (dots) compared to numerical solution of the ODE (traces), with parameters as in Fig. 3. Adjusting the simulation parameters to fit the data showed that all circuit parameters are within 3% of their expected values. The insets show the agreement of the (digitized) data and simulation near the fixed point.

diffusion rate is $\frac{A_0}{2}$ or

$$D = \left\langle \left(\frac{V_N}{V_2} \right)^2 \right\rangle \left(\frac{R_2}{R_4} \right)^2 \frac{T}{4R_1C_1}$$

in terms of the scaled variables used in Appendix B. The theoretical minimum diffusion constant for our circuit parameters given by eq. (B-1) is well below the intrinsic noise in the circuit. This intrinsic noise is not well characterized and occurs in both the x and y variables. We use a large enough value of the noise amplitude so that the intrinsic noise contribution is negligible. We show in Figs. 16 and 17 the quantities T_{n-1} vs x_n and T_n vs x_n , first obtained from the experiment and also by integrating numerically the differential equations with the same parameters, in particular $D = 4.7 \times 10^{-4}$. (These results are similar to those in Fig. 8, but with a different value of D .) The agreement is very good.

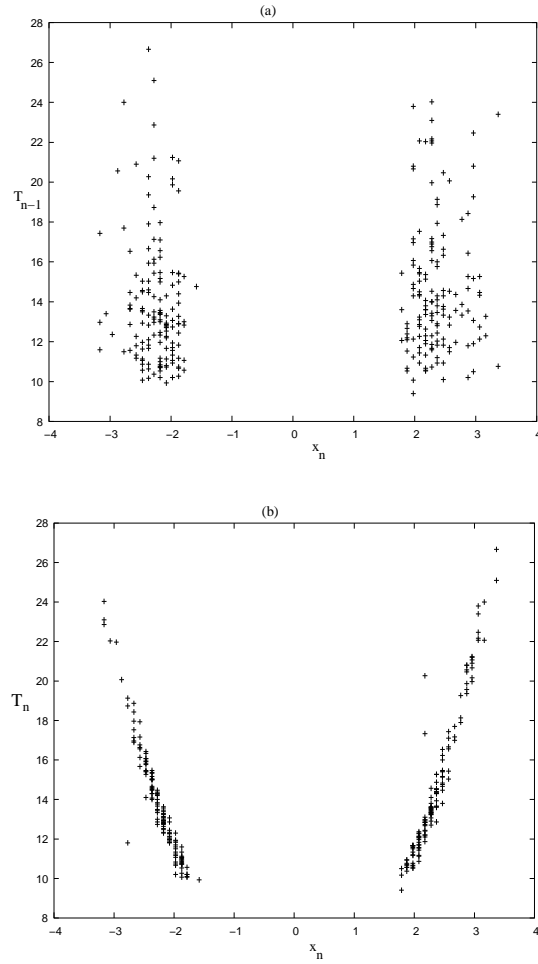


Figure 16: Comparison of peak height x_n to (a) time since previous peak T_{n-1} and (b) time until next peak T_n , from experiments. The correlations seen here are indicative of noise stabilization. The noise level is $D \simeq 4.7 \times 10^{-4}$.

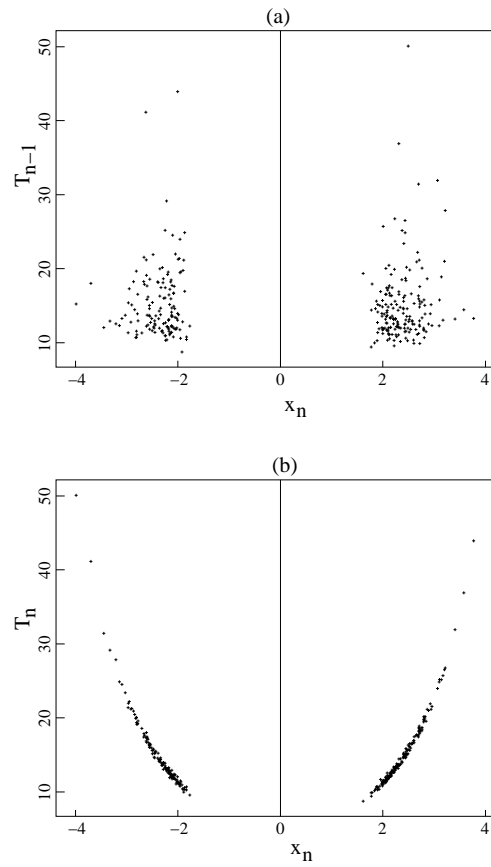


Figure 17: The same quantities as in Fig. 16 from numerical computation of eqs. (12), (13).

5.2 Offsets and symmetry breaking

The primary difficulty in designing this circuit is that small DC offsets at the input of the integrators significantly change the differential equations. In particular, an offset in the input to the y -integrator either drives the V_y -output negative to create an error in the AD538 computational unit, or it leads to a stable limit cycle similar to that described in Sec. 4.4. We adjusted a small current ($\sim 0.45\mu\text{A}$) to minimize the V_y -offset, using the automatic reset circuit to recover whenever V_y became negative. The reset kicks the circuit back into the vicinity of one of the unstable spirals. The x -integrator naturally follows, bringing V_x to a value near its fixed point. Without this reset, a negative value of V_y leading to the failure of the AD538 causes the circuit to fall to a stable fixed point with a large negative value of V_y . An external trigger can also reset the circuit to values near its unstable fixed point.

Similarly, we also corrected the offset in the x -integrator by adding $\sim 0.2\mu\text{A}$ at the integrator input. We adjusted this value until the noise signal generated equal numbers of negative and positive x pulses. After these adjustments, we observed the basic structure of the oscillations as they evolved away from the fixed point, in order to verify that the circuit waveforms were the same as the model calculations (see Fig. 15). The fact that such a simple adjustment can give results in agreement with the symmetric model is consistent with the extended concept of structural stability discussed at the end of Sec. 4.1. The results also show that the circuit is a sensitive detector of offsets.

6 Summary

We have performed a study of a nonlinear stochastic ODE whose deterministic form has unstable spirals, leading to bursty behavior, with successive bursts growing in magnitude and with larger time intervals between them. This bursty behavior is due to the fact that after each burst, the orbit comes closer to the unstable manifold (y -axis) of a hyperbolic fixed point at the origin, and therefore travels farther along this unstable manifold before diverging from it to form the next

burst.

In the presence of noise at a very small level, the bursts get stabilized in the sense of becoming limited in magnitude. The time interval between them also limited, and the bursts can go to either positive or negative x . In many qualitative senses, the behavior appears like deterministic chaos.

This system has reflection symmetry in x ; an offset a in x destroying this symmetry can lead to completely different behavior, depending on its magnitude relative to the noise. That is, the bursty behavior seen in the symmetric deterministic equations is not structurally stable. With noise and a small value of the offset $|a| < \sqrt{2D}$ (D is the Brownian diffusion coefficient), the bounded bursty behavior persists, but with more bursts going to the right if $a > 0$ (to the left if $a < 0$.) For larger offset $a \gtrsim \sqrt{2D}$, all bursts go to the right and basically give a noisy form of the stable limit cycle. In this sense, the results in the presence of noise and $a = 0$ are structurally stable.

We have considered modifications to the model allowing for saturation of y , because bursts cannot continue to grow without bound in a physical system. We have also considered modifications near the saddle at the origin, to give the saddle at the origin a positive eigenvalue. This change in the linear part of the flow near the saddle affects the time intervals between bursts, making their characteristic value much smaller, but does not affect the properties of the burst amplitudes, or the signs (in x) of the bursts.

We have described briefly results on a nonlinear circuit satisfying the same equations as the model. The circuit behaves similarly to the model. In particular, the circuit is very sensitive to the presence of an offset, and in practice the offset is adjusted to minimize the asymmetry of the signal. More details are presented in Ref. [17] and in Appendix B.

The system (12), (13) and its generalizations in Sec. 4 are arguably the simplest realizations of systems in which a small noise level can limit the amplitude of bursts and lead to qualitatively distinct behavior. We have listed in the Introduction physical examples of systems in which this effect may be important. For the tokamak example, the results here should have an impact on low dimensional modeling of ELMs. Indeed, the observation of chaotic time dependence of ELM data suggests that a simple autonomous ODE model must be three-dimensional. However, tokamaks

are known to have a broad spectrum of fluctuations (turbulence). If these fluctuations can be treated as uncorrelated noise, i.e. if their correlation time is much shorter than ELM time scales, it is justifiable to explore two-dimensional models with noise such as the models studied here.

Appendix A: Fokker-Planck Equation

The stochastic behavior of eq. (15) is governed by the Fokker-Planck equation for the probability density function $f(x, t)$,

$$\frac{\partial f}{\partial t} + \frac{\partial}{\partial x} (\gamma(t)xf) = \frac{\partial}{\partial x} \left(D \frac{\partial f}{\partial x} \right), \quad (\text{A-1})$$

where $D = \sigma^2/2$ is the diffusion coefficient. For arbitrary $\gamma(t)$, (A-1) has the exact solution

$$f(x, t) = \sqrt{\frac{1}{2\pi\alpha(t)}} e^{-x^2/2\alpha(t)}$$

if the variance or temperature $\alpha(t)$ satisfies

$$\frac{d}{dt}\alpha(t) = 2[\alpha(t)\gamma(t) + D]. \quad (\text{A-2})$$

Eq. (A-2) has the solution

$$\alpha(t) = 2D \int_{-\infty}^t ds_1 e^{2\int_{s_1}^t \gamma(s_2)ds_2},$$

assuming $\alpha(t \rightarrow -\infty) = 0$. Thus, $\alpha(t)$ is proportional to D , with a coefficient depending on $\gamma(t)$.

If γ is approximately constant ($|\dot{\gamma}/\gamma^2| \ll 1$) and negative, α approaches a slowly varying state with $\alpha(t) = D/|\gamma(t)|$, in which the inward motion due to the advective term in (A-1) balances diffusion and $\partial f/\partial t$ is negligible. This limit gives

$$f(x, t) \rightarrow \sqrt{|\gamma|/2\pi D} e^{-|\gamma|x^2/2D}. \quad (\text{A-3})$$

Another limit is recovered by neglecting $\gamma(t)$ in eq. (A-1), giving

$$\alpha(t) = \alpha(t_1) + 2D(t - t_1) = 2Dt + 2\alpha_0,$$

where t_1 is the time when $\dot{\gamma} \sim \gamma^2$. Without loss of generality we can set the time where $\gamma = 0$ to $t = 0$. This range, in which the advective term in eq. (A-1) is small, gives the purely diffusive random walk result

$$f(x, t) \sim \frac{1}{\sqrt{4\pi(Dt + \alpha_0)}} e^{-x^2/4(Dt + \alpha_0)}. \quad (\text{A-4})$$

A third range has γ positive with advection dominating diffusion. We find

$$\alpha(t) = \alpha(t_2) \exp\left(2 \int_{t_2}^t \gamma(s) ds\right), \quad (\text{A-5})$$

where t_2 is the time this range is entered, i.e. where $\gamma(t_2)\alpha(t_2) \sim D$. In this range the noise becomes negligible.

A simple example having these properties has γ linear in time, $\gamma(t) = \dot{\gamma}_0 t$. Again taking $\alpha(t = -\infty) = 0$, we find

$$\alpha(t) = 2D e^{\dot{\gamma}_0 t^2} \int_{-\infty}^t e^{-\dot{\gamma}_0 s^2} ds.$$

In this example $\alpha(t)$ has slow growth for $t < t_1 \equiv -1/\sqrt{\dot{\gamma}_0}$, diffusive increase for $t_1 < t < t_2$, where $t_2 = 1/\sqrt{\dot{\gamma}_0}$, and exponential growth for $t > t_2$. The value of $\alpha(t)$ at $t = 0$ (corresponding to $y = 1$) is $\sigma_x^2 \equiv \alpha(0) \sim D/\sqrt{\dot{\gamma}_0}$.

For application to eqs. (12), (13), consider x small so that its equation is linear (when the second term on the right in (13) is negligible). We then note that if α is small for $y \approx 0$, then $\alpha(t)$ near $y = 1$ (recall $\gamma(t) = y(t) - 1 = 0$) is proportional to $D/\sqrt{\dot{\gamma}_0}$. Since $\dot{\gamma} = \dot{y} \sim \epsilon$, we have $\alpha(y \approx 1) \sim D/\sqrt{\epsilon}$. After a diffusive stage, α continues to increase as in eq. (A-5), with noise no longer playing a role. Thus, the nonlinear orbit for later times depends only on the noise accumulated by the time (here $t = t_2$) just after the orbits cross the throat at $y = 1$; the value of x at $y \approx y_2$, when noise last plays a role, is proportional to $\sqrt{\alpha} \propto D^{1/2}/\epsilon^{1/4}$. See Fig. 10. Thus, in

essence, the orbit from the crossing of $y = 1$ with small x out to the next crossing and back to near the origin is deterministic, and the noise plays its role only along the y -axis.

Appendix B: Circuit Design

The design of our circuit is basically the same as reported in Ref. [17], but we have adjusted our circuit parameters, and extended the analysis of the circuit behavior. For the sake of completeness, we have included all of the new circuit parameters in this appendix, as well as our analysis of the minimum noise amplitude necessary to keep the circuit from saturating the circuit elements.

The analog circuit consists of three basic sub-circuits: the x -integrator, the y -integrator, and the reset controller, as shown in Fig. 18. The integrators use OPA 4228 operational amplifiers (low noise, 33 MHz bandwidth) with capacitive feedback (10 nF) to integrate their inputs. V_1 and V_2 are constant applied voltages, while V_x and V_y are time varying voltages, proportional to $x(\tau)$ and $y(\tau)$, respectively.

The input to the y -integrator uses an AD538 real-time computational unit (400 kHz bandwidth) to raise the V_y voltage to a fractional power, $V_y(t)^{\nu-1}$, by taking its logarithm, scaling the result by $\nu - 1$, and then exponentiating to generate $V_1(V_y(t)/V_2)^{\nu-1}$. This output is then added into the output of an MPY634 precision multiplier (10 MHz bandwidth) that creates the ratio $V_x^2(t)/V_2$. A second MPY634 multiplies this combined signal by V_y/V_2 before it enters the integrator. We also use additional small adjustable current sources to eliminate offsets.

The input to the x -integrator is the sum of V_x , the noise source, and $V_x V_y/V_2$ formed by another MPY634. The net output signal of the entire circuit has a maximum frequency of 2 KHz, well within the bandwidth limit of all the components. This circuit does the following integrations:

$$\begin{aligned} V_x(t) &= V_x(t_0) + \int_{t_0}^t \left(\frac{R_2 V_y(t')}{R_3 V_2} - 1 \right) V_x(t') \frac{dt'}{R_2 C_2} + \int_{t_0}^t V_N(t') \frac{dt'}{R_4 C_2}, \\ V_y(t) &= V_y(t_0) + \int_{t_0}^t \left(V_1 \left(\frac{V_y(t')}{V_2} \right)^\nu - \left(\frac{V_x(t')}{V_2} \right)^2 V_y(t') \right) \frac{dt'}{R_1 C_1}, \end{aligned}$$

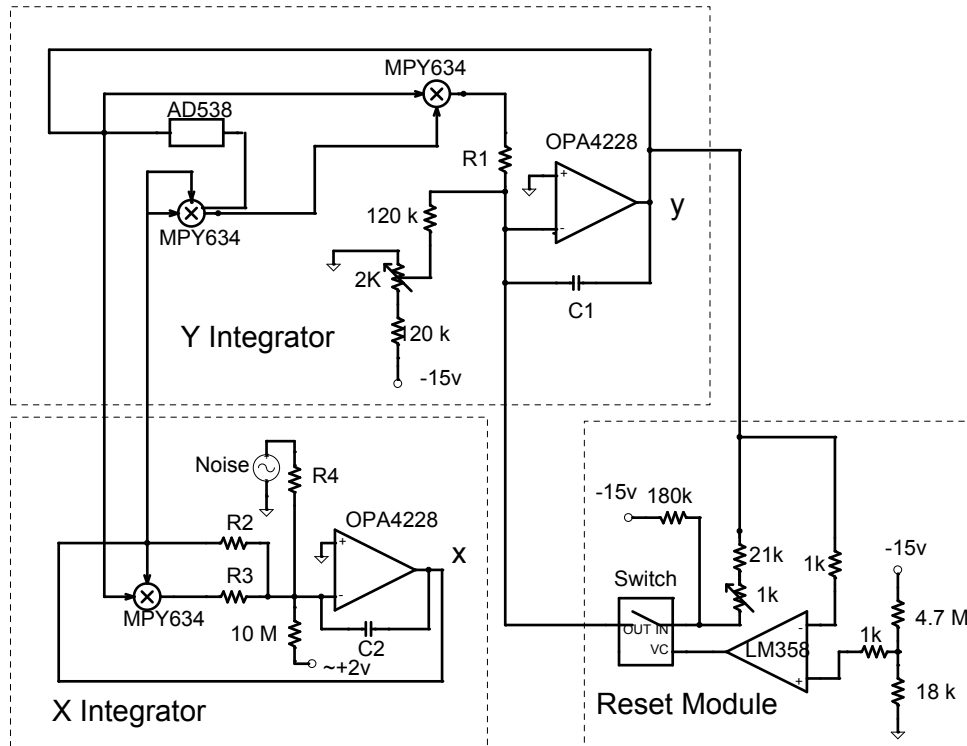


Figure 18: Circuit diagram.

where the circuit components had the values listed in Table 1, and the parameter $\nu - 1$ was set to 0.2 in the AD538 component by a voltage divider composed of a 2200 Ω resistor and a 560 Ω resistor. This dimensional form of the equations is related to the dimensionless form by defining x , y , τ , ϵ and η as:

$$\begin{aligned} y &= \frac{R_2 V_y}{R_3 V_2} \\ \tau &= \frac{t}{R_2 C_2} \\ \epsilon &= \frac{R_2 C_2 V_1}{R_1 C_1 V_2} \left(\frac{R_3}{R_2} \right)^{\nu-1} \\ x &= \sqrt{\frac{R_2 C_2 V_x}{R_1 C_1 V_2}} = \sqrt{\epsilon} \frac{V_x}{\sqrt{V_1 V_2}} \left(\frac{R_2}{R_3} \right)^{\frac{\nu-1}{2}} \\ \eta &= \sqrt{\frac{R_2 C_2 V_N R_2}{R_1 C_1 V_2 R_4}} \end{aligned}$$

This leads to fixed points at:

$$\begin{aligned} V_{y*} &= \frac{R_3}{R_2} V_2 \\ V_{x*} &= \sqrt{V_1 V_2} \left(\frac{R_3}{R_2} \right)^{\frac{\nu-1}{2}} \end{aligned}$$

Thus, a circuit design with a given value of ϵ has its fixed points and its voltage scaling determined by the choice of the ratio R_3/R_2 . This value can be optimally set by forcing both the x circuit and the y circuit to reach saturation values on the same cycle. For the $\nu = 1$ case, neglecting the logarithmic terms of the Hamiltonian $H(x, y)$ in eq. (3), the peak value of y (y_p) and its following peak value of x (x_p) are related by $x_p^2 = 2y_p$ if H is large enough, i.e. for bursts with x_p , y_p large enough. These two peak values cannot require voltages in excess of V_2 , or the multipliers will fail, and the peaks will be clipped. To optimize, we equate these peaks when they reach V_2 ; for the $\nu = 1$ case this gives $\epsilon V_2/V_1 = 2R_2/R_3$ or, for our values of V_1 and V_2 ,

$$\frac{R_2}{R_3} = \frac{\epsilon V_2}{2 V_1} = 6.25.$$

This choice then implies maximum values of $x_m = \sqrt{2(\epsilon V_2/2V_1)} = 3.53$, and $y_m = \epsilon V_2/2V_1 = 6.25$. These maximum values of x and y determine the minimum noise amplitude that must be

V_1	$0.4V$
V_2	$10V$
R_1	$6.8k\Omega$
R_2	$122k\Omega$
R_3	$19.5k\Omega$
R_4	$67k\Omega$
C_1	$10nF$
C_2	$10nF$

Table 1: Values of circuit elements.

present to keep the voltage peaks within the operating range of the multipliers. The logarithmic dependence observed in Fig. 11 can be approximated as $\langle x \rangle = (1/8) \ln(10^5/D)$, so that:

$$D_{min} = 10^5 e^{-8x_m} = 10^5 e^{-8\sqrt{2\left(\frac{\epsilon V_2}{2V_1}\right)}} \sim 2 \times 10^{-10}. \quad (\text{B-1})$$

When the amplitudes are low enough to avoid clipping, the measured results are in agreement with those given in Sec. 3.2.

ACKNOWLEDGMENTS

We wish to thank C. Doering, J. Guckenheimer, E. Ott, and D. Sigeti for valuable discussions. This work was supported by the U. S. Department of Energy, under contract W-7405-ENG-36, Office of Science, Office of Fusion Energy Sciences, and by the NSF-DOE Program in Basic Plasma Physics under contract PHY-0317256.

References

- [1] H. Zohm, Plasma Phys. Contr. Fusion **38**, 105 (1996).
- [2] J. W. Connor, Plasma Phys. Contr. Fusion **40**, 191 (1998).
- [3] X. D. Shi, M. P. Brenner, and S. R. Nagel, Science **265**, 5169 (1994).
- [4] C. Liu *et al.*, Physical Review E **55**, 6483 (1997).
- [5] D. Sigeti and W. Horsthemke, J. Stat. Phys. **54**, 1217 (1989).
- [6] E. Stone and P. Holmes, SIAM J. Appl. Math. **50**, 726 (1990).
- [7] E. Stone and D. Armbruster, Chaos **9**, 499 (1999).
- [8] D. Armbruster, E. Stone, and V. Kirk, Chaos **13**, 71 (2003).
- [9] J. Moehlis, Phys. Lett. A **284**, 172 (2001).
- [10] L. Billings and I. Schwartz, J. of Math. Bio. **44**, 31 (2002).
- [11] E. Bollt, L. Billings, and I. Schwartz, Physica D **173**, 153 (2002).
- [12] S. H. Strogatz, *Nonlinear Dynamics and Chaos* (Westview Press, Cambridge, MA, 1994).
- [13] E. Ott, *Chaos in Dynamical Systems* (Cambridge University Press, Cambridge, UK, 2002).
- [14] T. M. Cover and J. A. Thomas, *Elements of Information Theory* (Wiley, New York, 1991).
- [15] G. M. Odell, in *Mathematical Models in Molecular and Cellular Biology*, edited by L. A. Segel (Cambridge University Press, Cambridge, UK, 1980), Chap. "Qualitative theory of systems of ordinary differential equations, including phase plane analysis and the use of the Hopf bifurcation theorem." Appendix A.3.
- [16] J. M. Finn *et al.*, Chaos **13**, 444 (2003).

- [17] W. E. Cooke *et al.*, in *Proceedings of the 8th Experimental Chaos Conference* (AIP Conference Proceedings 742, Melville, New York, 2004), p. 63.